Collaborative design and analysis of Electro-Optical sensors

Jason Geis, Jeff Lang, Leslie Peterson, Francisco Roybal, David Thomas
The Aerospace Corporation
2350 E. El Segundo Blvd
El Segundo, CA 90245

INTRODUCTION

Complex products are best developed in a collaborative design environment where engineering data and CAD/CAE results can be shared across engineering discipline boundaries within a common software interface. A new software tool that allows Electro-Optical (EO) sensors to be developed in this manner has been used to conduct an integrated Structural/Thermal/Optical (STOP) analysis of a critical lens subassembly in a flight payload. This paper provides a description of the software environment and a summary of the technical results that were produced with it.

THE TRADITIONAL EO SENSOR DESIGN PROCESS

A number of engineering disciplines (mechanical, structures, thermal, optics, electronics, software) are needed to design and build modern Electro-Optical (EO) sensors. Separate design models are normally constructed by each discipline engineer using the CAD/CAE tools and material properties familiar to each discipline. Design and analysis are conducted largely in parallel subject to requirements that have been levied on each discipline, and technical interaction between the different engineering disciplines is limited and infrequent. Design reviews are also conducted in a serial manner and by engineering discipline using PowerPoint snapshots of design and analysis status. Access to engineering results is largely limited to discipline specialists because of the level of education and experience needed to understand the technical issues, terminology, and computer tools needed to do discipline work.

A unified view of the sensor design across engineering discipline boundaries is not directly possible in this traditional approach, and generating one would require a separate, largely manual, and error-prone process. For these reasons, the discovery of sensor-level design issues tends to occur late in the design process, often after the hardware has already been built. Late discovery of design issues, when they are far more time consuming and expensive to fix, has been identified as a key contributor to the rise in on-orbit failures and large (100% or more) cost and schedule overruns that currently affect a quarter of civil and security space EO sensor programs [Refs 1-3].

A COLLABORATIVE EO SENSOR DESIGN ENVIRONMENT

A number of software tools have been developed over the past ten years or so that promote a more integrated approach to product design across engineering discipline boundaries for a variety of applications. A Simulation Driven Engineering (SDE) software tool suitable for the collaborative design of EO sensors has been developed by Comet Solutions, Inc. (http://www.cometsolutions.com). This SDE software has the following useful attributes (see Figure 1):

1. All engineering data (material properties, boundary conditions, meshing parameters, etc.) and CAD/CAE simulation results are stored and viewed within a common software environment without needing to know how to run the underlying CAD/CAE tools of each of the engineering disciplines.
2. Project data is organized in a tree structure that captures design history and ensures version control.
3. Top-level summary data (mass, image quality metrics, key parameter values) are extracted from the detailed design and displayed in a “dashboard” area for review by engineering, system engineering, and management personnel.
4. Expertise for complex, interdisciplinary analyses can be developed by discipline engineers and captured for reuse as a Simulation Process, dramatically reducing the design cycle time needed for repeating those analyses as the design evolves and matures.

5. The SDE software works in concert with other Commercial Off The Shelf (COTS) engineering software through adapters that allow the discipline engineers to conduct their detailed work with the same CAD/CAE tools that they already use to do their everyday work. The environment may also be extended to include additional applications, including cost and schedule tools, by developing new adapters for those applications.

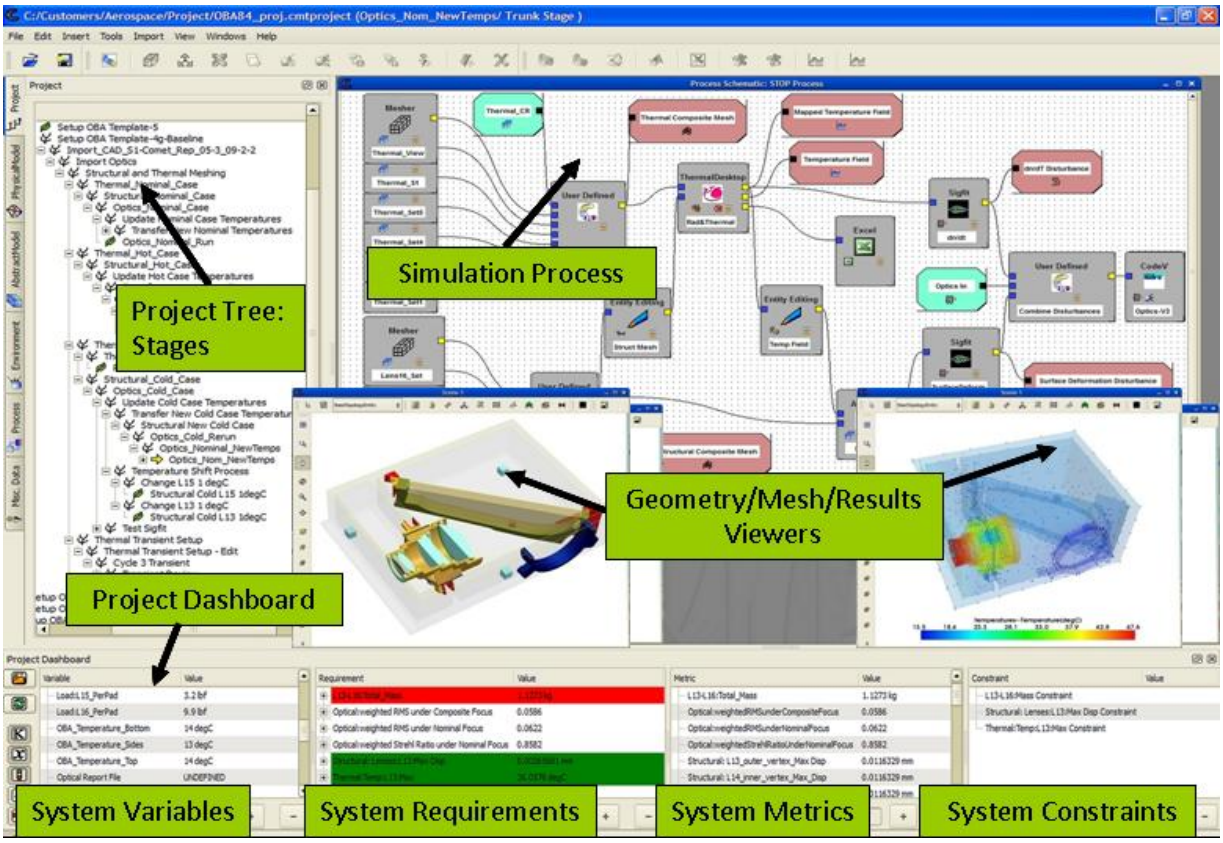

Figure 1: The SDE Software Interface

INTEGRATED STRUCTURAL/THERMAL/OPTICAL (STOP) ANALYSIS

A small, interdisciplinary engineering team from The Aerospace Corporation has recently used the SDE software environment to conduct an independent Structural/Thermal/Optical (STOP) analysis of a critical lens subassembly (L13-16) in the visible channel of a space flight payload. STOP analysis evaluates the changes in sensor focus and image quality that arise from the structural deformations and refractive index changes that occur in a space-borne optical system when the thermal environment of the sensor changes throughout its orbit. This STOP model was used to validate an unconventional focus control approach that was being used by the instrument contractor to maintain focus for the visible channel over its expected thermal environment. STOP analyses were conducted for six different test conditions applied during final thermal vacuum (TVAC) testing of the payload on the ground.

The STOP Simulation Process shown in Figure 2 was used to conduct the integrated STOP assessment of the contractor's focus control method. The STOP process begins with importing a single integrated CAD model of the instrument geometry into the SDE software environment. Independent thermal and structural meshes are then generated. The thermal mesh and relevant engineering data for material properties and thermal boundary conditions are used to compute temperature distributions at nodal points in both the thermal and structures mesh within Thermal Desktop (http://www.crtech.com), a COTS thermal design and analysis code. Thermally induced structural deformations of the metering structure and optical components are then evaluated in Abaqus (http://www.simulia.com), an industry standard code for structural design and analysis. Thermal and structural results are next imported into SigFit (http://www.sigmadyne.com), another COTS tool that computes best fit rigid body displacements for the optical surfaces

and Zernike polynomial representations for wavefront errors introduced by refractive index changes (dn/dT) in the lens components and deformations of the lens surface figures. SigFit creates a modified lens subassembly (L13-16) optical prescription that is imported into CODE V (http://www.opticalres.com) for evaluation of optical performance impacts. Some more detail on each of these process steps is given below.

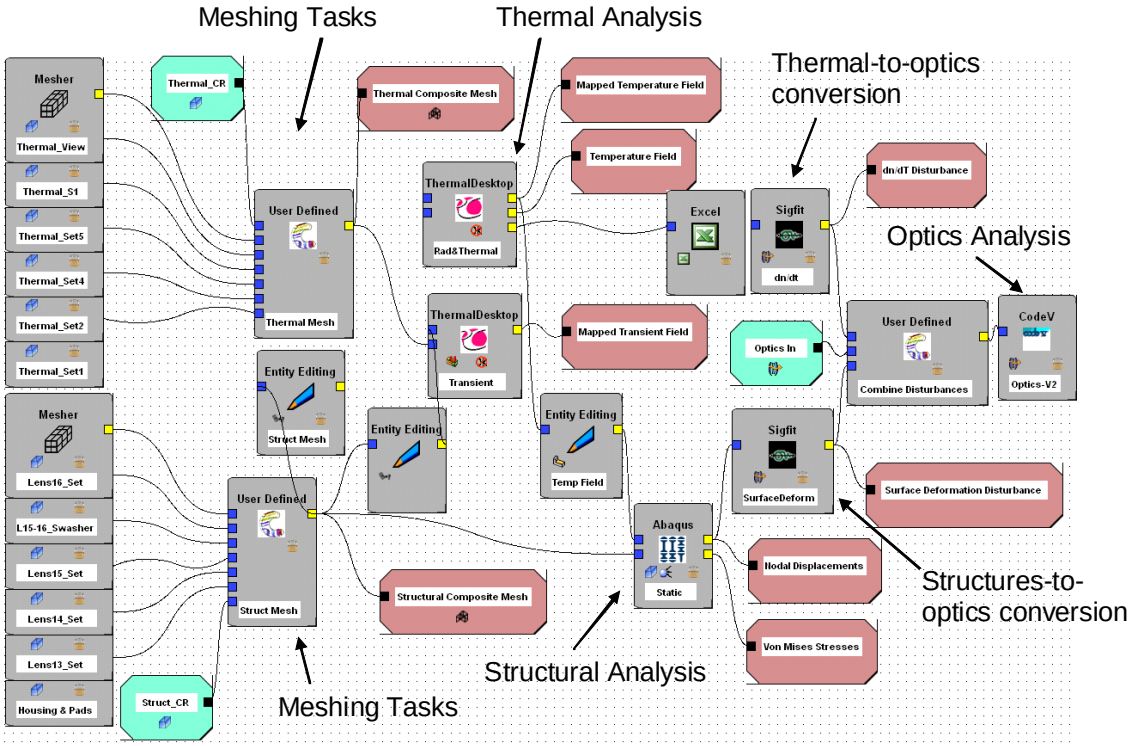

Figure 2: Integrated STOP Simulation Process

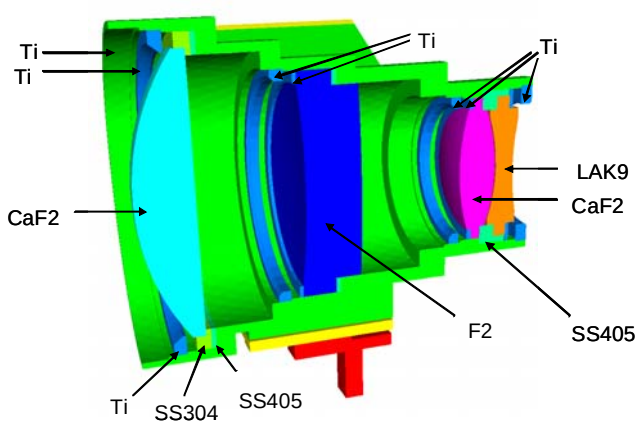

Figure 3: Tagged CAD model

The integrated STOP process begins by importing a single integrated CAD model for the optical assembly into the mechanical CAD application, Pro/E (http://www.ptc.com). Tags are applied by discipline engineers to the parts, faces, and subassemblies that they will use for downstream analysis using an SDE software plug-in. Tags are used to apply a variety of properties to the CAD model and to re-apply those properties when either they or the CAD model itself are changed as trade studies or design alternatives are explored. CAD geometry is tagged to group parts for meshing, set meshing parameters, identify optical surfaces, and associate material properties and surface treatments with parts and surfaces, for example (Figure 3).

L13-16 Thermal mesh

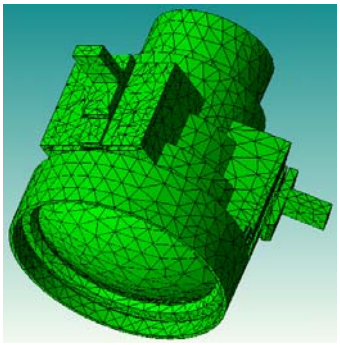

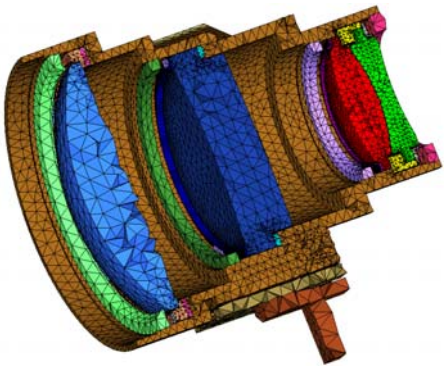

L13-16 Structures mesh

Figure 4: Thermal and Structures analysis meshes

After the CAD model is imported and tagged, the thermal and structures engineers develop Finite Element Meshes (FEM) for the parts of the CAD model that are of interest to them for subsequent analysis. Meshing parameters are developed and iteratively refined by each discipline to produce computationally efficient yet stable results, and these parameters are captured for re-use at each stage of design evolution within the SDE software environment (Figure 4).

The thermal model consists of the thermal mesh for the system geometry plus all of the conditions and properties needed to evaluate the distribution of temperatures across the optical system. The thermal and optical properties of all materials, heater power levels, boundary condition temperatures, and conductances between the various components that make up the thermal model are all specified within an engineering data model in the integrated environment. This data model is, among other things, a database of engineering data for all of the engineering disciplines that can be shared and re-used by any of the underlying applications. For any given TVAC test condition of interest, the above thermal model parameters are passed to Thermal Desktop for computation of temperatures at each node on the thermal mesh. Thermal Desktop is also used to map these temperatures onto the nodes in the structures mesh.

Similarly, the structures model consists of the structures mesh for the system geometry plus all of the conditions and properties needed to evaluate the structural deformations produced in response to the temperature field calculated by Thermal Desktop. The structural properties of all materials, boundary conditions, and assumptions about the types and parameters of structural contact between components are specified in the integrated data model. These parameters and the structures mesh are passed to Abaqus for computation of displacements of each node in the structures mesh.

The temperatures and displacements at the nodes on the structural mesh are passed to a pair of SigFit tasks using the SDE software adapter developed for that purpose. One of the SigFit tasks computes the best fit rigid body displacements and tip/tilt of each lens surface and a set of Zernike polynomials that represents the aperture-dependent lens surface deformations, including radius of curvature change, for each surface. The other task computes a single set of Zernike polynomials for each lens component that represents aperture-dependent wavefront errors introduced by thermally-induced refractive index changes within the lens. SigFit uses this information to generate a modified lens design sequence file that it passes to CODE V through an SDE software adapter interface for subsequent analysis of optical performance impacts. For the purposes of this STOP analysis, the thermally distorted L13-16 CODE V prescription was substituted into the nominal overall telescope prescription to look for changes in visible channel image quality and focus due only to L13-16 lens subassembly effects (Figure 5).

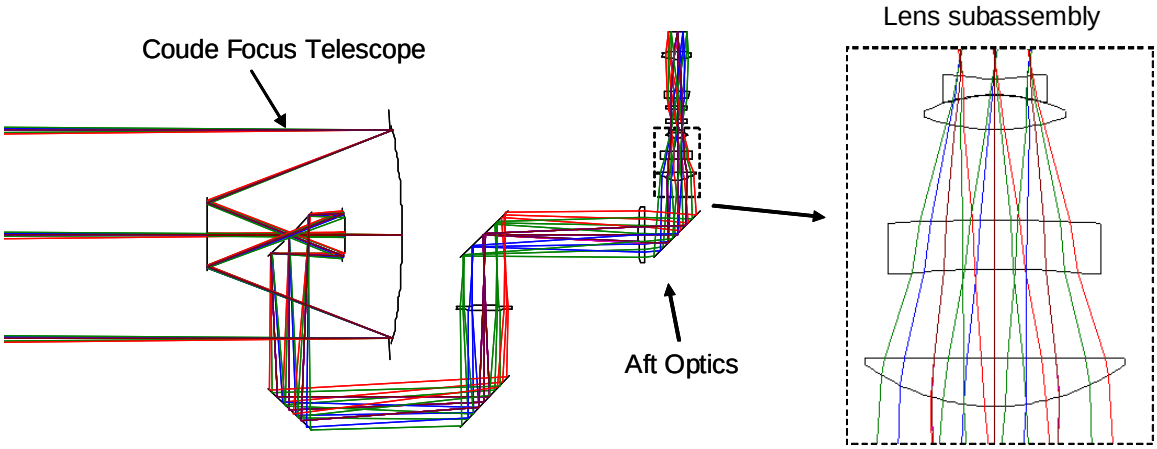

Figure 5: Optical design model

VALIDATION OF THE INTEGRATED STOP THERMAL MODEL

The thermal model developed for our integrated STOP analysis was validated using test data from a special test configuration constructed by the instrument contractor. For this test, an engineering model L13-16 lens subassembly was instrumented with extra thermocouples and subjected to thermal soak and thermal transient tests while mounted by three stainless steel standoffs inside of a 42-inch diameter thermal vacuum chamber. Figure 6 shows a plot that compares our model predictions to measured thermocouple values at the inside and outside surface vertices of lens 13 for the transient thermal test. Our model predictions were in excellent agreement with measured values for three different lens heater conditions.

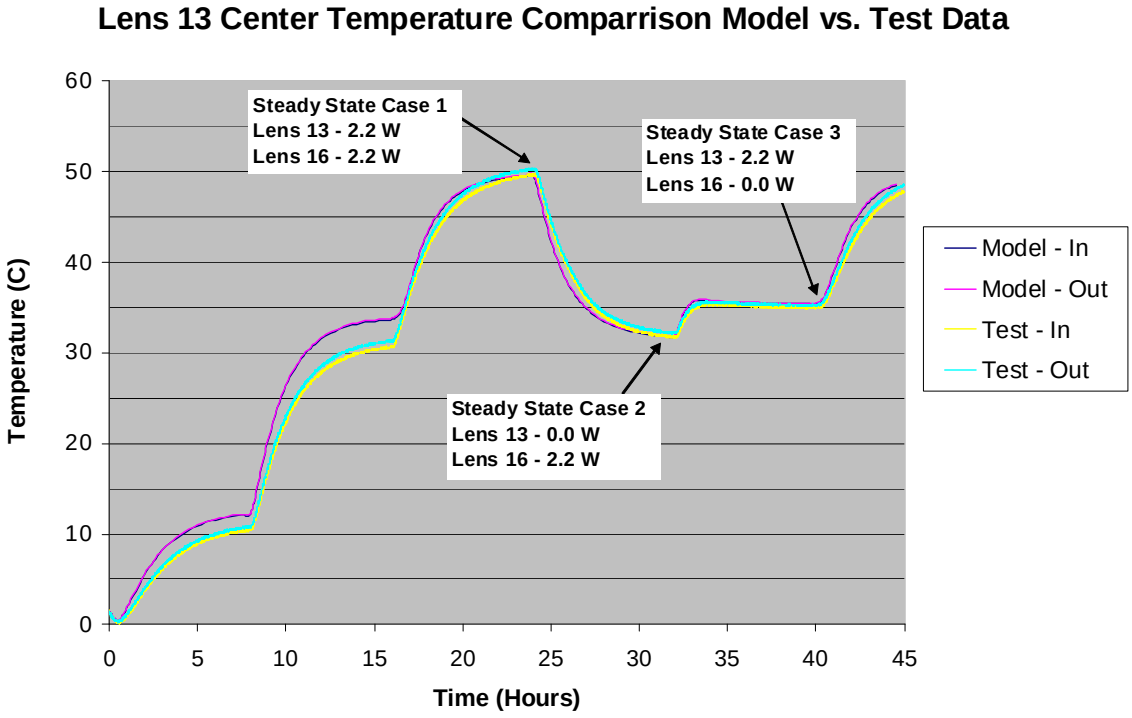

Figure 6: 42-inch chamber thermal transient test results

Thermocouple	Comet Model (°C)	Test Data (°C)	Comet Model □T
L13_F_S1	49.5	50.5	-1.0
L13_F_C	49.3	49.7	-0.4
L13_F_S2	49.5	49.8	-0.3
L13_B_S1	49.6	50.7	-1.1
L13_B_C	49.4	50.3	-0.9
L13_B_S2	49.6	50.8	-1.2
L14_F_S1	56.1		
L14_F_C	55.9	55.3	0.6
L14_F_S2	56.3	56.2	0.1
L14_B_S1	56.8	57.0	-0.2
L14_B_C	56.7	56.9	-0.2
L14_B_S2	56.6	58.4	-1.8
L15_F_S1	63.6		
L15_F_C	63.5		
L15_F_S2	63.6	61.6	2.0
L15_B_S1			
L15_B_C			
L15_B_S2			
L16_F_S1			
L16_F_C			
L16_F_S2			
L16_B_S1	58.1	52.6	**5.5**
L16_B_C	57.0	52.1	**4.9**
L16_B_S2	58.2	50.5	**7.7**
H_L13_R1	59.7	60.3	-0.6
H_L13_R2	59.1	51.2	**7.9**
H_L13_R3	59.5	57.7	1.8
H_SOH_R1	57.7	59.4	-1.7
H_SOH_R2	57.1	58.2	-1.1
H_SOH_R3	57.2	59.8	-2.6
H_L16_R1	65.9	63.7	2.2
H_L16_R2	65.8	48.7	**17.1**
H_L16_R3	65.8		

Table 1: 42-inch chamber thermal soak test comparisons

A comparison of our model predictions to measured thermocouple data at all available monitoring points for a thermal soak test condition is given in Table 1. Results correlate very well with test data for most thermocouples. Predictions for lens 16 are higher than test results by 5C to 8C. The largest (7.7C) discrepancy is in part due to a questionable test data reading, as the periphery of the lens (50.5C) should never be cooler than the center of the lens (52.1C) when heat is applied to the outside lens barrel. Some of the lens 16 model predictions may be in error due to the fidelity of our model of the support structure used for this test (standoff feet, etc.). Lens 16 has the largest view of this structure of all of the lens elements. Significant differences between model predictions and measured data are also observed for two of the lens barrel thermocouples (H_L13_R2 and H_L16_R2). These differences are thought to be due to anomalies in the measured data. The R2 thermocouple readings are much lower than their partner R1 and R3 readings, and our model shows that gradients this large should not appear along the perimeter of the metal housing. These thermocouples may not have been bonded well enough to get a good reading, or they may have been placed in locations that were not as close to the heated areas of the housing as expected.

INTEGRATED STOP MODEL PREDICTIONS FOR THERMAL SOAK TESTS

The CAD model for the portion of the visible optics channel analyzed for this report is shown in Figure 7. The sensor was subjected to three separate thermal soak test conditions – a hot case, a nominal case, and a cold case. For each test, state of health thermocouple readings from several points on the optical bench (OBA) and applied heater powers for L13-16 were supplied by the instrument contractor during final thermal vacuum testing of sensor performance. This data was imported into our integrated environment via an Excel spreadsheet, and the STOP process shown in Figure 2 was executed.

STOP analysis results are given below for the cold soak test condition. Figure 7 shows the distribution of temperatures computed across the overall thermal mesh for the entire visible channel model. Figure 8 gives the distribution of temperatures calculated for the L13-16 subassembly, the axial thermal gradients computed for the lens components alone, and a typical radial thermal gradient distribution calculated for lens 13. The axial component of the structural node displacements computed subject to the temperature distributions shown in Figure 8 are given in Figure 9. The temperature fields and structural displacements are used to compute the best fit rigid body displacements and wavefront error contributions for each lens in the L13-16 subassembly. Figure 10 shows some of this data for lens 13. Finally, a

ray trace and diffraction analysis is conducted for the entire visible channel optics prescription with the distorted L13-16 prescription substituted for the nominal L13-16 design to obtain exit pupil wavefront and system MTF data (Figure 11).

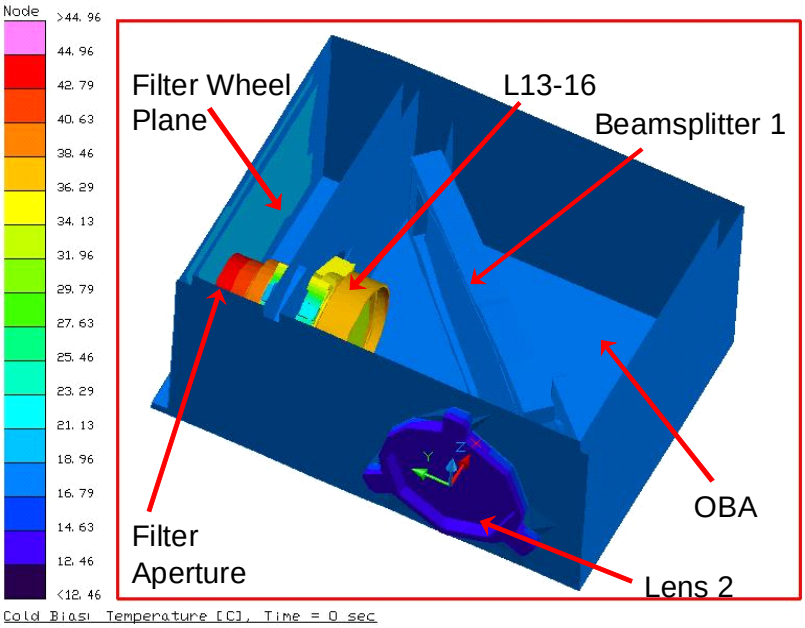

Figure 7: Visible channel CAD model

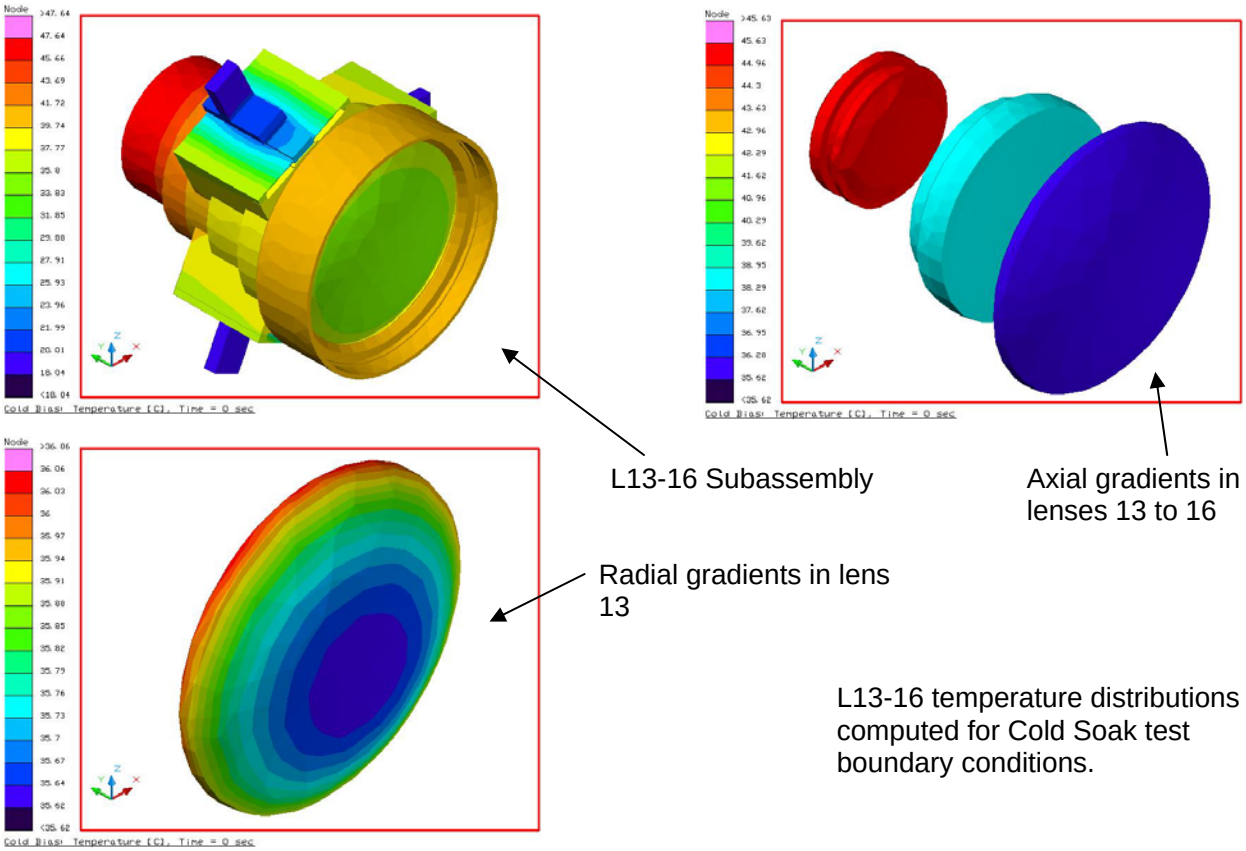

Figure 8: Cold soak L13-16 temperature predictions

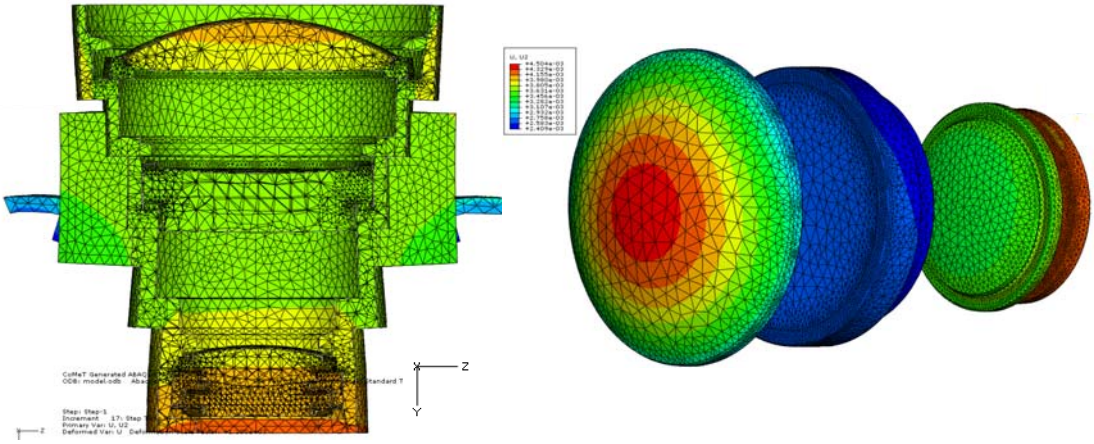

Figure 9: Cold soak structural axial displacements

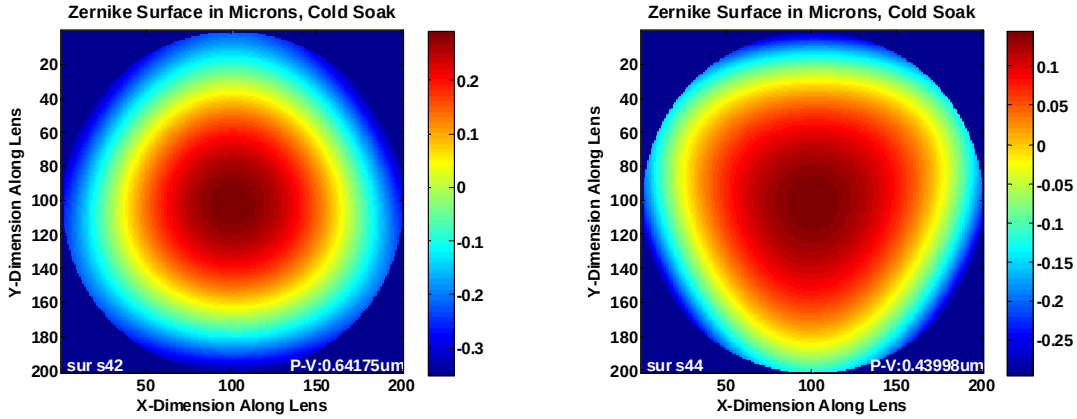

Wavefront error, entry surface of lens

Wavefront error, exit surface of lens

x-decenter	S41	6.14E-05 in	Best fit rigid body displacements of lens surfaces computed by SigFit.	x-decenter	S42	6.17E-05 in
y-decenter	S41	2.43E-05 in		y-decenter	S42	2.56E-05 in
z-decenter	S41	1.87E-04 in		z-decenter	S42	1.21E-04 in
a-tilt	S41	1.17E-04 °		a-tilt	S42	1.19E-04 °
b-tilt	S41	-2.91E-05 °		b-tilt	S42	-4.23E-05 °
c-tilt	S41	-5.79E-04 °		c-tilt	S42	-5.79E-04 °

Figure 10: Lens 13 surface wavefront error contributions and best fit rigid body displacements

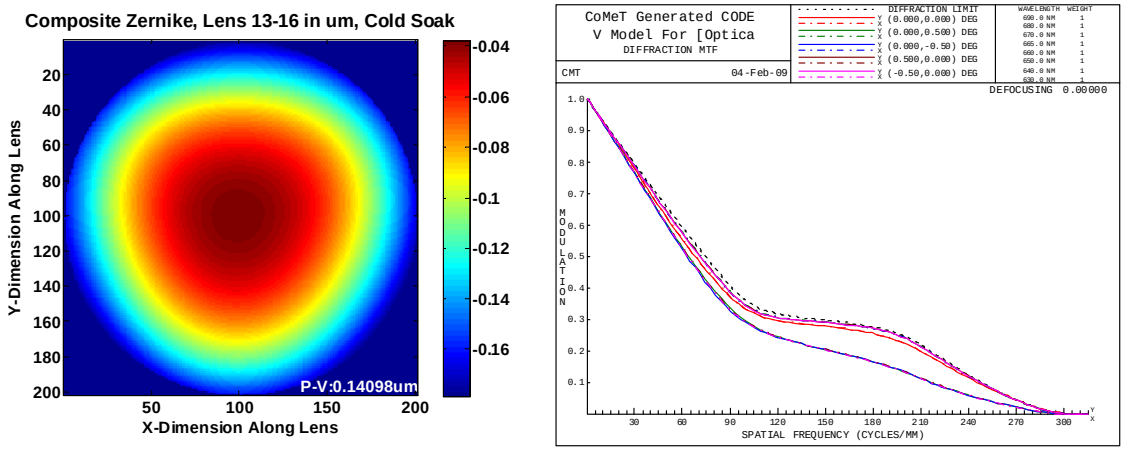

Figure 11: Cold soak visible channel wavefront error and Modulation Transfer Function (MTF)

INTEGRATED STOP MODEL ANALYSIS FOR THERMAL TRANSIENT TESTS

Following the thermal soak tests, the payload was subjected to a series of periodically varying thermal cycles designed to simulate the transient thermal environment that the payload will see on-orbit. Profiles of boundary condition temperatures and applied L13-16 heater power for the third of these cycles are shown in Figure 12. Three integrated STOP analyses were conducted using data from the thermal transient tests in the following manner. Starting from an average initial L13-16 temperature distribution for cycle 3, temperature distributions were computed within Thermal Desktop for a 1230 minute period, with temperature outputs recorded every 30 minutes. Three time slices were extracted through the SDE software interface to map temperatures onto the structures mesh for STOP analysis at 600 minutes (hot case), 930 minutes (nominal case), and 1230 minutes (cold case). Results similar to those shown in Figures 8 through 11 were computed for each of these three cases.

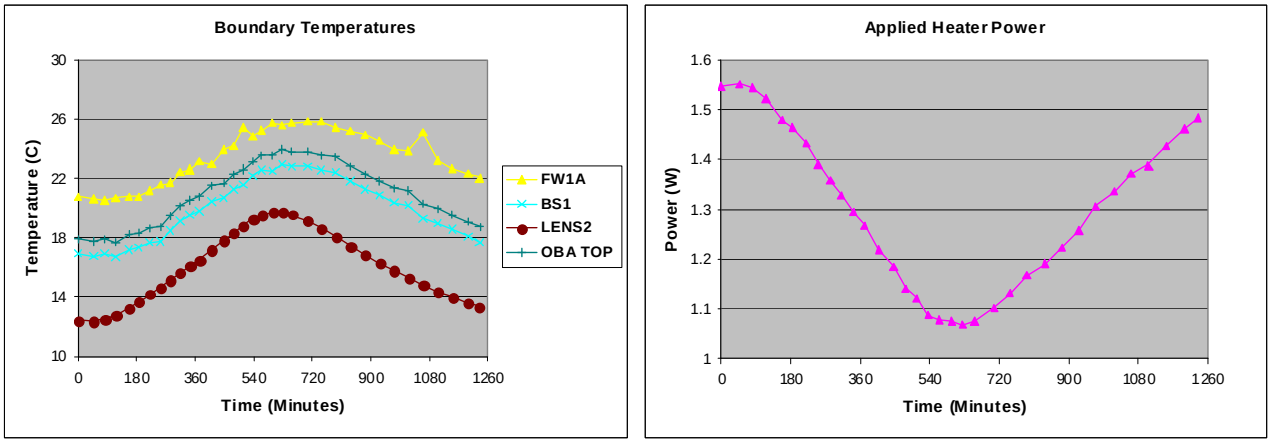

Figure 12: Thermal transient test boundary condition and heater power profiles

INTERPRETATION OF TECHNICAL FINDINGS

Our integrated STOP analysis results for both the thermal soak and the thermal transient test data may be understood and interpreted with the help of the summary data provided in the following three tables. Table 2 provides some key parameters for the thermal focus control system for the hot and cold cases in each test. These data show that at least for applied heater powers above 1 watt, the applied heater power needed to maintain focus is roughly proportional to the

difference in temperature between the surrounding optical bench and the L13-16 set point temperature. Note that the L13-16 set point temperature is not the same as the design bias temperature of 41C. The set point temperature is chosen by the instrument contractor's control algorithm as the value best suited to maintain focus for the environmental boundary condition temperatures of interest. Note also that the size of the axial thermal gradient that is set up in the lens components 13 to 16 is roughly proportional to the applied heater power.

	Thermal Soak Hot Case	Thermal Soak Cold Case	Thermal Transient Hot Case	Thermal Transient Cold Case
Bench Temp (C)	36.7	17.5	22.5	17.7
L13-16 Temp (C)	39.3	36.6	37.0	37.0
L13-16 – Bench (C)	2.6	19.1	14.6	19.3
Heater power (W)	0.24	1.46	1.08	1.48
Axial gradient (C)	2.1	10.0	7.6	10.2

Table 2: Thermal control system parameters

Table 3 summarizes the changes from nominal 41C design residual values in lens component wavefront error contributions predicted by the integrated STOP analyses for the same four test conditions. Wavefront errors are given in terms of Peak-to-Valley (PV) magnitudes in waves at a 0.6328 micron wavelength. Here we see that the two calcium fluoride lens elements (13 and 15) dominate, and that the wavefront error increments from lenses 13 and 15 tend to compensate for one another at all heater power levels.

	Thermal Soak Hot Case	Thermal Soak Cold Case	Thermal Transient Hot Case	Thermal Transient Cold Case
L13 dn/dT WFE	-0.31	-0.98	-0.86	-0.77
L13 surface WFE	0.35	1.71	1.51	1.32
L14 dn/dT WFE	0.01	0.03	0.03	0.03
L14 surface WFE	-0.01	0.00	0.00	0.00
L15 dn/dT WFE	0.01	0.36	0.14	0.40
L15 surface WFE	-0.19	-0.82	-0.45	-0.91
L16 dn/dT WFE	0.00	-0.06	-0.03	-0.07
L16 surface WFE	0.03	0.13	0.07	0.15

Table 3: Changes in lens component wavefront error contributions with heater power level

Our integrated STOP analysis provides the following physical insight into the operation of this unconventional thermal focus control approach. The further the surrounding optical bench temperature falls below the 41C design bias temperature for L13-16, the more heater power is applied to the strip heaters at the lens 13 and lens 16 ends of the lens subassembly to hold focus for the visible channel. Equal heat is applied to both ends of the L13-16 subassembly, setting up both an axial thermal gradient from L13 to L16 and smaller radial thermal gradients within each lens. The two CaF2 lens elements (13 and 15) have lower nominal refractive indices than the glass elements (14 and 16), but much larger dn/dT values. At all heater power levels, the additional wavefront errors that are introduced by lenses 13 and 15 dominate, indicating that thermally induced refractive index changes are driving changes in optical performance. The radial gradients set up in the lenses are small ($1/3^{rd}$ to $1/10^{th}$) compared to the changes in the average bulk temperature of each lens, so bulk temperature changes in the lenses have the dominant effect on image quality. Lens surface figure changes due to retaining spring stresses on the optical surfaces were also evaluated in our integrated STOP analysis, but

were found to produce negligible wavefront error contributions. The L13-16 set point temperatures selected by the instrument contractor's control algorithm always results in raising the temperature of the smaller diameter lens 15 CaF2 element above the 41C design bias temperature and lowering the temperature of the larger diameter lens 13 below the design point so that the thermally induced wavefront error contributions for these two lenses always tend to cancel one another for all heater power levels. This tends to leave the total focus and image quality contributions for the L13-16 subassembly relatively unchanged over the expected thermal environment of the sensor.

The overall effectiveness of this thermal control approach in maintaining focus and visible channel wavefront error is shown by the data summarized in Table 4. Our analysis verified that the instrument contractor's focus control approach for the visible channel is, to first order, effective at maintaining focus over the expected temperature range of the sensor. The aberration residual for each test condition is within the diffraction limit (0.25 waves PV) for all cases but one (transient, hot case). Further, that aberration residual may be removed by an additional refocus of the amount indicated in Table 4 for each test case. Except for the transient hot case, these refocus values are within the instrument contractor's error budget allocation for defocus due to thermal effects (1 mil).

	Soak WFE (P-V at HeNe)	Soak refocus	Transient WFE (P-V at HeNe)	Transient refocus
Baseline Design	0.03	N/A	0.03	N/A
Hot case	0.18	-0.3 mils	0.26	-1.4 mils
Nominal case	0.10	-0.1 mils	0.12	0.6 mils
Cold case	0.22	-0.5 mils	0.08	-0.1 mils

Table 4: Focus control effectiveness

CAVEATS TO OUR INITIAL STOP ANALYSIS

The fidelity and overall utility of our initial integrated STOP analysis were limited by three factors. First, we were not able to directly compare STOP model image quality predictions to measured image quality for the sensor visible channel due to limitations in the baseline optical design model that was used for our analysis. Our optical design model included only the baseline optical design and a simplified representation of the central obscuration in the sensor. It did not include fabrication, alignment, or gravity release errors, which are significant for this sensor. It also did not include the significant aberrations of the collimator that was used to test the sensor. This limitation will be addressed in future work by adding a Zernike phase surface to the baseline design that represents these errors. Second, our STOP model was of high fidelity for the L13-16 lens subassembly, but of limited fidelity for the rest of the visible channel due to time and computing resource limitations. Small errors in the overall tilt and decenter of the L13-16 subassembly may have been introduced due to the limited fidelity of our structural model of the optical bench, and optics performance impacts due to visible channel components other than L13-16 were ignored. These limitations will be addressed according to the needs of our customer for follow-on work. Finally, the accuracy of the thermal transient optics predictions was affected by two factors. An average initial temperature distribution was used for L13-16 rather than computing its evolution from its initial condition over the previous two thermal cycles due to time and computing resource limitations. There may have been some small errors in the temperature distributions used for STOP analysis for this reason. More importantly, the temperature and therefore the focus of the all-aluminum collimator that was used to test the payload was not controlled during thermal transient testing, so some of the focus shift observed in these tests, especially for the extreme temperature conditions, may have been due to drifts in collimator focus over time and with temperature. This is a limitation in the test setup that may need to be corrected if the test is ever repeated.

CONCLUDING REMARKS AND PLANS FOR FUTURE WORK

A new commercial SDE software environment for the integrated design and analysis of Electro-Optical sensors has been used to validate an unconventional thermal control approach for maintaining focus of the visible channel of a flight payload over its expected thermal environment. Both flight hardware measurements and our integrated STOP analysis showed that the approach works to at least first order. Two additional benefits were derived from our integrated analysis methodology. First, it provided superior physical insight into how the thermal control approach works and hence how to further improve the small residual focus errors that remain. Second, the integrated STOP process that we developed allows an interdisciplinary analysis that formerly took several days or weeks to perform to be completed in a single day. The savings in cost and schedule required to perform this independent assessment due to this dramatic reduction in design cycle time were substantial given that six different integrated STOP analyses were required to complete this work.

Further work is planned to support On-Orbit Testing (OOT) of this payload and final thermal vacuum testing of a second payload. Our baseline optical design model will be updated to include fabrication, alignment, and gravity induced effects, and more of the visible channel components will be added to the model to allow higher fidelity comparisons of predicted and measured visible channel image quality. We also plan to add an adapter to the SDE software environment so that the controls algorithm software may be included in the integrated analysis. This will allow the entire focus control system to be modeled from ground command through final image quality.

REFERENCES

[1] Pavlica, Steve and William Tosney, “Assessment of NRO Satellite Development Practices,” The Aerospace Corporation, 2003.

[2] Young, Thomas A., Chair, “Report of the Defense Science Board/Air Force Scientific Advisory Board Joint Task Force on Acquisition of National Security Space Programs,” Office of the Under Secretary of Defense for Acquisition, Technology, and Logistics, May 2003.

[3] NASA Instrument Capability Study, Final Report, NASA Office of the Chief Engineer, NASA Headquarters, December 2008.

[4] Panthaki, Malcolm, “Concurrent Engineering to the Rescue: Do We Have the Software Tools to Support It?” Proc SPIE, Vol. 7071, 3 September 2008.